ACS Biomaterials SCIENCE & ENGINEERING

Article

Cite This: ACS Biomater. Sci. Eng. 2018, 4, 2784−2793

Wettability Study on Natural Rubber Surfaces for Applications as Biomembranes

Rodney Marcelo do Nascimento,*[,†] Stella M. M. Ramos,[‡] Ivan Helmuth Bechtold,[§] and Antônio Carlos Hernandes[†]

[†]São Carlos Institute of Physics, University of São Paulo, Avenida João Dagnone, 1100, Jardim Santa Angelina, CEP 13563-120, São Carlos, SP, Brazil

[‡]Institut Lumière Matière, UMR5306 Université Claude Bernard Lyon 1-CNRS, Université de Lyon, 43 Boulevard du 11 Novembre 1918, 69100, Villeurbanne, France

[§]Departamento de Fisica, Universidade Federal de Santa Catarina. Campus Reitor João David Ferreira Lima, s/n, Trindade, CEP 88040-900, Florianopolis, SC, Brazil

Supporting Information

ABSTRACT: This manuscript reports an experimental study on surfaces of natural rubber membranes modified by incorporation of calcium phosphate particles. In particular, we focused on the wettability, a subject for biological aspects. Five surfaces of natural rubber (NR) membranes (pure, polymer-bioceramic composite (NR-CaP), and three modified surfaces subjected to a simulated body fluid (NR-SBF)) were produced and characterized by confocal Raman-spectroscopy, AFM, SEM, and XPS, and the results were correlated with the wetting properties. Seven liquids (water, formamide, di-iodomethane, ethylene glycol, hexadecane, simulated body fluid, and human blood droplets) were used in different experimental sections. Static and dynamic contact angle measurements were conducted to obtain the solid−liquid tensions, work of adhesion, and depinning forces. The incorporation of CaP particles in the polymer decreases the roughness and increases the interfacial adhesion, and there was no dependence between the morphology and equilibrium contact line. The hydrophobic state of the NR surfaces is preserved. After exposure to a biological environment, the NR surfaces were chemically modified increasing blood wettability and decreasing the negative surface charges and the contact angle to values close to those associated with protein adsorption and cell adhesion, therefore opening possibilities for applications of these materials as biomembranes. On the other hand, the concepts applied, regarding different wettability aspects, should enable the evaluation of biomaterial surfaces and provide new insights allowing a better understanding of body fluid−material interfaces.

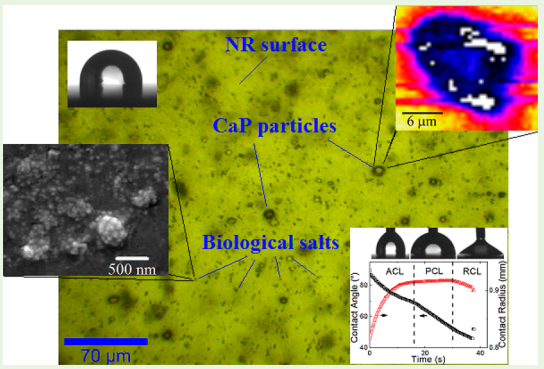

KEYWORDS: *natural polymer, body fluids, contact angle, contact line, blood stain ring*

1. INTRODUCTION

Hybrid polymers used in biomedical implantable devices[1] for the treatment of bone defects around implants need to be able to withstand biological environments and exhibit cell affinity. An ideal biomaterial for applications as occlusive membranes or bone adhesives provides an adequate surface-biological interface for the formation of a natural framework of fibrins, i.e., an optimized bone tissue precursor.[2] Natural polymers associated with bioactive materials, such as natural rubber NR-calcium phosphate composite NR-CaP,[3] are potentially attractive for such applications. Due to its flexibility, renewability, and biocompatibility,[4] NR is an interesting option for guided bone regeneration.[5,6] However, the surface properties, a key element for biointerface applications, remain undescribed, or at least limited, because of several evident constraints. For instance, no study has focused on the wetting properties of the NR surface after incorporation of the drugs since the biomedicine is a promising field for application of the NR-based materials. Both the topology and morphology of the surfaces are important parameters to be considered for the biomaterial. On the other hand, the wetting regimes of the blood on NR surfaces are unknown and a good understanding of the relation between morphology and wettability (fluid mobility, adhesion, etc.) is required for the applications of NR as a biomaterial interface.

Phenomenological studies on the wettability of biomaterials are important to both the fundamental and applied sciences. Many of these have addressed the wetting properties focusing on biological and clinical aspects[7−10] and on the cell response.[11−13] The physical mechanisms of the wettability

Received: June 26, 2018
Accepted: July 10, 2018
Published: July 10, 2018

DOI: 10.1021/acsbiomaterials.8b00723
ACS Biomater. Sci. Eng. 2018, 4, 2784−2793

are responsible for the optimization of the tissue regeneration through cell seeding, proliferation, and new tissue formation in three dimensions, showing great promise in tissue engineering research. A decade ago, studies showed that the suitability of a biomaterial can be attributed to the adsorption of proteins with a correlated water droplet contact angle, which should lie within the range of 30° to 60°.[14] Despite the ultralow contact angle inhibiting the cell response,[15] cell adhesion generally tends to be favored on hydrophilic surfaces, whereas cell detachment tends to be favored on hydrophobic surfaces.[16] On the other hand, the cell response is strongly influenced by the free surface energy,[17,18] surface charge,[15,19] topology,[18,20] and roughness[21,22] after the initial contact between body fluids and the surface of the implant. Therefore, great efforts are required to improve our understanding of the role of the wettability on biomaterials, due to the complexity, heterogeneity, and dynamics of the interface. The following hypothesis still need to be tested: the contact line behavior, with regard to phenomena occurring at interfaces, such as capillary penetration,[23] pinning−depininng,[24] and stain ring effects,[25] is a function of the modification of the NR surface by the biological environment.

This manuscript reports an experimental study on the interfacial phenomena and surface properties of the natural rubber membranes aiming at applications as biomaterials. Section 3.1 outlines the surface features of the NR and NR-CaP with regard to the morphology, topography, and chemical structure. Section 3.2 addresses the wettability of surfaces through static and dynamic contact angle measurements for the determination of interfacial tension and pinning−depinning forces. Section 3.3 introduces the NR samples modified by a biological environment, with different atomic concentrations on their surfaces. Section 3.4 describes the monitoring of the contact line behavior through the evaporation dynamics of the sessile drop. Lastly, section 3.5 addresses the blood wetting as well as the stain ring effects of the evaporated blood droplets as a function of the hybridization of the NR surface. The results should provide new insights regarding phenomena associated with body fluid−natural rubber interfaces.

2. EXPERIMENTAL SECTION

2.1. Materials. Natural rubber samples collected from *Hevea brasiliensis* trees were immediately transferred to propylene tubes containing ammonium hydroxide at 2% (volume) and stored under refrigeration at 4 °C to avoid microbial contamination. The samples underwent a centrifugation process for the separation of the cream phase. This phase was then dried at 60 °C and slowly dissolved in chloroform until it reached a viscous gel state at room temperature. The final soft material was a polymeric matrix, and this was used to design the membranes of 40 × 20 × 0.3 mm^3 fixed on glass and silicone substrates. The membranes were subjected to a thermal treatment at 40 °C in a laminar flow cabinet for 24 h for the complete elimination of the solvent. The following three surfaces of NR membranes were obtained for the studies: pure natural rubber, composite natural rubber with incorporation of calcium phosphate particles (cell viability on CaP coatings was described elsewhere by our group[15]), and natural rubber modified by exposure to simulated body fluid (SBF). The samples were labeled NR, NR-CaP, and NR-SBF, respectively.

2.2. Liquids. Ultrapure water (γ^p = 51 $mN{\cdot}m^{-1}$, γ^d = 21.8 $mN{\cdot}m^{-1}$, and γ = 72.8 $mN{\cdot}m^{-1}$) was used in all wettability experiments, i.e., characterization in the body temperature range, dynamic wetting, and evaporation kinetics (where γ denotes liquid surface tension and γ^p and γ^d are polar and dispersive components of γ, respectively).

Formamide (γ^p = 18.5 $mN{\cdot}m^{-1}$, γ^d = 39.5 $mN{\cdot}m^{-1}$, and γ = 58 $mN{\cdot}m^{-1}$), ethylene glycol (γ^p = 19 $mN{\cdot}m^{-1}$, γ^d = 29 $mN{\cdot}m^{-1}$, and γ = 48 $mN{\cdot}m^{-1}$), di-iodomethane (γ^p = 0 $mN{\cdot}m^{-1}$, γ^d = 50.8 $mN{\cdot}m^{-1}$, and γ = 50.8 $mN{\cdot}m^{-1}$), and hexadecane (γ^p = 0 $mN{\cdot}m^{-1}$, γ^d = 27.47 $mN{\cdot}m^{-1}$, and γ = 27.47 $mN{\cdot}m^{-1}$) were added for the determination of the solid tension γ_S and solid−liquid tension γ_{SL}.

Simulated body fluids[26] were used to obtain the NR-SBF samples. The surfaces were exposed to a biological environment for different periods of time, i.e., 1, 15, and 30 days (samples denoted as NR-SBF#1, NR-SBF#15, and NR-SBF#30n, respectively) at pH ∼ 7.4 and 36 ± 1 °C. All experiments were conducted with triplicate samples. After each period, the samples were gently cleaned in ultrapure water and dried in an aseptic ambient chamber.

Droplets of blood were evaporated on the NR surfaces modified in the biological environment. Human blood from a healthy volunteer was collected in a São Francisco analysis center and stored in sterile tubes with anticoagulant. Experiments were performed within 5 h of donation to avoid deterioration of the liquid. Data on the evaluation of the blood samples are available in the Supporting Information. Blood droplets (1 μL) were evaporated at 36 ± 0.5 °C to simulate the conditions in the body and ensure the same surface tension. The protocols were approved by the ethics committee of the institution with national registry of health (CNES) n° 5901995.

2.3. Physical and Chemical Characterization of the Surfaces. The physical and chemical characterization of the surfaces was carried out at the *Sao Carlos Institute of Physics* (IFSC) of the *University of Sao Paulo* (USP, Brazil) with collaboration from the *Analysis Center* of the *Federal University of Ceará* (UFC) and Laboratório de Físico-Química de Superfícies e Colóides, Departamento de Química-FFCLRP of the University of Sao Paulo. Topographical and morphological analyses of the surfaces were performed by atomic force microscopy (AFM) on Shimadzu SPM instrument (version 2.0). Statistical data on the surface area were obtained from different regions of each sample and are provided in the Supporting Information.

Raman spectra for the NR and NR-CaP were acquired on a WITec *alpha* 300 system equipped with a linear piezo-driven scan stage, Nikon 20x and 100x objective lens, and a polarized laser operating at 632 and 514 nm. The Raman light was detected by a high-sensitivity back-illuminated spectroscopic CCD behind a 600 groove/mm grating. The integration time for each point was 0.5 s.

The modification of the surfaces after exposure to a biological environment for different periods was monitored by scanning electronic microscopy (SEM). Multiscale SEM images were obtained on a Quanta 450 (FEI) microscope with a field emission gun (FEG) operating at 10 keV equipped with a 100 mm stage and X-ray detector model 150.

The chemical heterogeneity of the surfaces after exposure to a biological environment was quantified by X-ray photoemission (XPS). X-ray spectra were obtained on a Scienta Omicron ESCA + spectrometer system equipped with an E A125 hemispherical analyzer and an Xm 1000 monochromated W-ray source in Al Kα (1486.7 eV) operating at 200 W power in a constant pass energy mode of 50 eV. The samples required the use of a Cn10 Omicron charge neutralizer with a beam energy of 1.6 eV and an emission current of 2 A in order to compensate the charge effects.

The charge effects of the membranes before and after modifications were investigated by surface zeta-potential (ζ) at pH 7.4. The values were measured on a Zeta-sizer Nano ZS instrument (Malvern Instruments) coupled to a ZEN 1020 dip cell. The mobility of tracer particles in the vicinity of the charged test surface fixed in the dip-cell was measured by using phase analysis light scattering and a simple model that describes the electroosmotic flow near the surface. The tracer particles consisted of polystyrene nanospheres (200 nm and ζ = −50.0 mV, Duke Scientific Corporation) dispersed in Milli-Q water. The measurements were repeated three times for each sample, at 25 °C. The samples were designed no larger than 7 × 4 × 1 mm^3. Statistical data on the surface charge are provided in the Supporting Information.

DOI: 10.1021/acsbiomaterials.8b00723
ACS Biomater. Sci. Eng. 2018, 4, 2784−2793

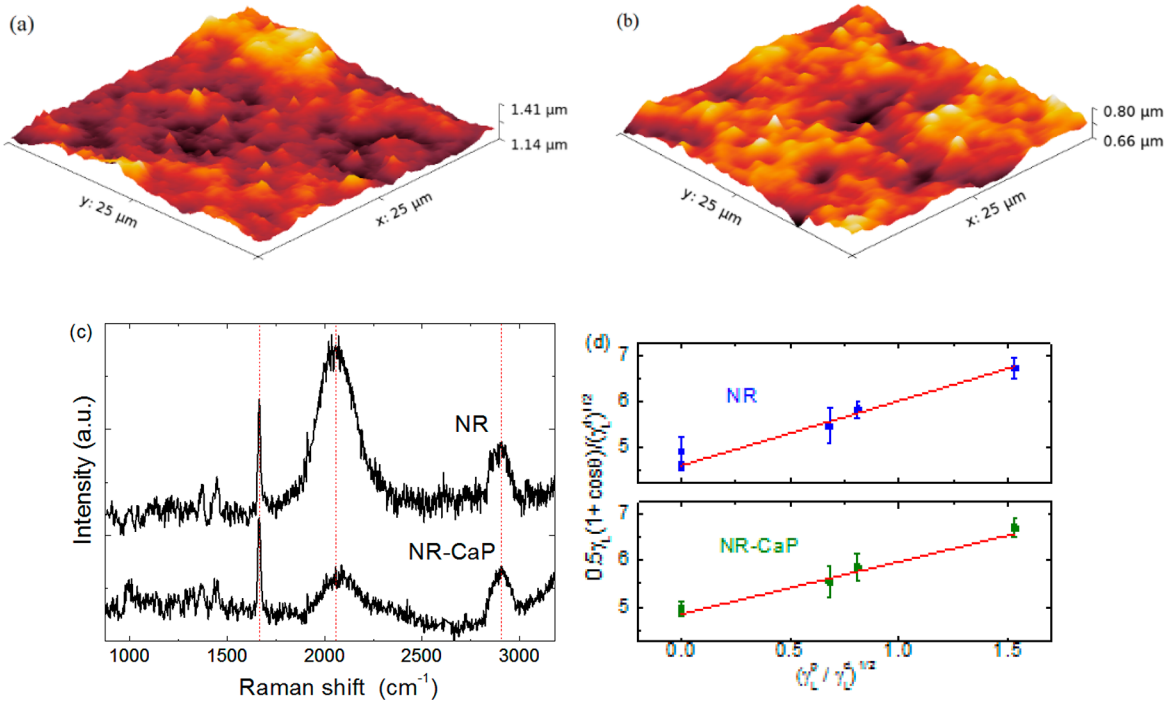

Figure 1. Physical and chemical characterization of NR surfaces before and after the incorporation of CaP particles: (a, b) AFM micrograph showing 3D view; (c) Raman spectra of characteristic peaks obtained with λ = 632 nm; (d) Plot of $0.5\gamma_L(1 + \cos\theta)(\gamma^d_L)^{-1/2}$ versus $(\gamma^p_L/\gamma^d_L)^{1/2}$ for the determination of dispersive γ^d and polar γ^p components from linear and angular coefficients of free surface energy.

Table 1. Roughness Parameters R_a (average) and R_{rms} (root mean squared), Equilibrium Contact Angle (θ) at 20, 37, and 54 °C, Advance Contact Angle θ_a, Recede Contact Angle θ_r, Rupture Contact Angle θ_{rup}, Solid−Liquid Tension γ_{SL}, and Work Adhesion at Interfaces W[a]

	R_a (nm)	R_{rms} (nm)	θ at 20 °C (deg)	θ at 37 °C (deg)	θ at 54 °C (deg)	θ_a (deg)	θ_r (deg)	θ_{rup} (deg)	γ_{SL} (mN m^{-1})	W (mJ·m^{-2})
NR	29	37	98 ± 2	90 ± 2	84 ± 2	69 ± 1	52 ± 4	45 ± 5	23.29	119
NR-CaP	15	20	98 ± 1	90 ± 1	85 ± 2	70 ± 2	–	23 ± 8	24.78	135

[a]The values of θ_a, θ_r, θ_{rup}, γ_{SL}, and W were obtained at 37°C, with $\gamma_L \cos\theta = 0$ and $\gamma_{SL} = \gamma_S$.

2.4. Wetting Characterization. Static contact angle measurements of liquid droplets (volume ~3 μL) were carried out at the *Sao Carlos Institute of Physics* (IFSC) of the *University of Sao Paulo* (USP, Brazil) through the standard sessile drop method on a KSV CAM 200 tensiometer/goniometer to obtain the solid tension γ_S. At least five measurements were taken in different areas of each sample. The resulting static contact angles for the calculation of γ_S are provided in the Supporting Information.

The dynamic contact angles and the evaporation dynamics of liquid droplets on natural rubber membranes were determined at the *Institut Lumière Matière* (ILM) of the *University of Lyon 1* (France). A device constructed in the laboratory was used for these experiments, allowing the substrate temperature and humidity rate to be controlled independently. The samples are introduced into a glass chamber, and the liquid drop is gently deposited on the substrate by an automatic injection pump. In order to simulate the temperature values in the oral environment, the substrates were heated to three different temperatures (20 °C, 37 °C, and 54 °C).

The three-phase contact line of the ultrapure water drop was advanced or receded by adding or withdrawing a small volume (~2 μL) of fluid. The steady-state advancing (θ_a) and receding (θ_r) contact angles were measured, allowing the determination of the dynamic contact angle hysteresis defined as $\Delta\theta_{dyn} = \theta_a - \theta_r$. The rupture angle θ_{rup} was measured immediately before the rupture of the meniscus (see snapshots for the three configurations in the inset of the graphical abstract). To avoid perturbation from external flux, the chamber remained closed during the experiments.

For the investigation of the evaporation kinetics, the same experimental device was used. In this part of the experiment, contact-angle measurements of the liquid drops were carried out through the standard sessile drop method. The static contact angle θ_i was measured immediately after the drop deposition of a drop on the surfaces investigated (NR, NR-CaP, and NR-SBF). Side-view images of the drops were recorded with a CCD camera for subsequent contact angle and contact radius measurements. The measurements were performed optically with an accuracy of 1°, on at least three drops deposited at different locations on each sample.

3. RESULTS AND DISCUSSION

3.1. Physical and Chemical Characterization of NR and NR-CaP Surfaces. We investigated the physical−chemical characteristics of the natural rubber with a view to its application as a biointerface (occlusive membranes, adhesive, coatings, etc.). Figures 1(a) and (b) show AFM micrographs of the NR and NR-CaP surfaces, respectively. The presence of bioceramic particles in the polymeric matrix significantly decreases the surface roughness parameters (see Table 1). In a previous study, NR membranes were prepared with different solvents, which showed that the volatility does not influence the surface morphology.[27] No significant molecular change was detected in the NR after the CaP incorporation, as attested by electrical permittivity measurements (ε = 2.2 ± 1.5 in the 1 to 10^6 Hz range). Therefore, the

DOI: 10.1021/acsbiomaterials.8b00723
ACS Biomater. Sci. Eng. 2018, 4, 2784−2793

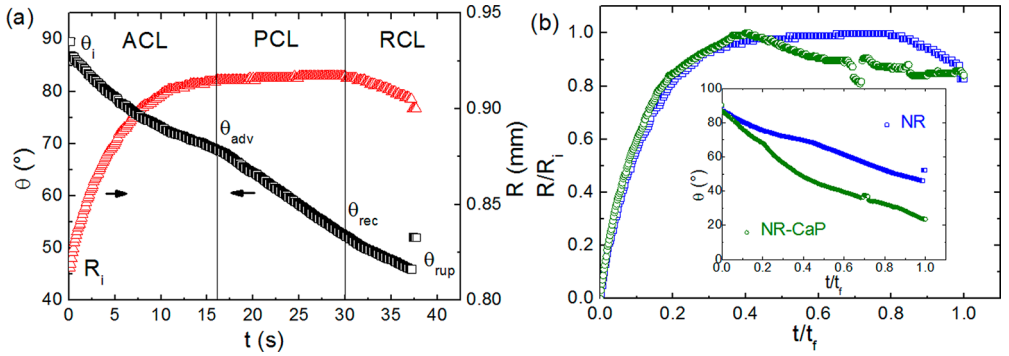

Figure 2. (a) Evolution of contact angle θ (red) and contact radius R (black) during the expansion and contraction of droplets. The measured advancing and receding contact angles are indicated; (b) Evolution of normalized contact radius R/R_i as a function of normalized time t/t_f measured for NR and NR-CaP surfaces at 37 °C. Inset: Evolution of contact angle θ.

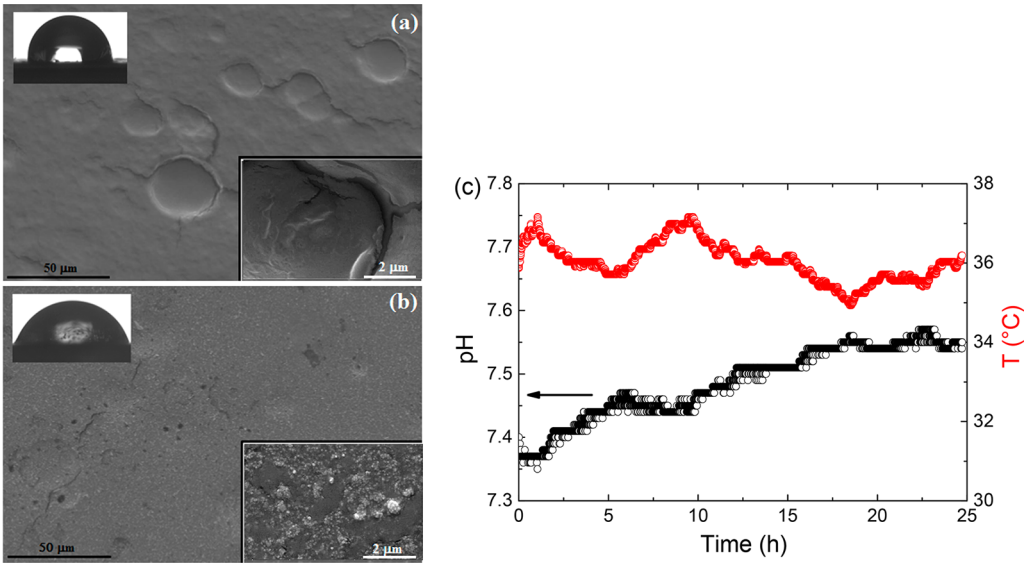

Figure 3. Scanning electron microscopy images of surfaces of natural rubber NR (a) and modified natural rubber surfaces after exposure to simulated body fluid NR-SBF (b). Insets: respective profiles of drops on NR (θ = 90°) and NR-SBF (θ = 60°). (c) Evolution of the pH and temperature of the SBF around the NR sample over 1 day of the incubation process.

presence of CaP particles may facilitate the dissolution and induce a better accommodation of the polymeric matrix during the solvent evaporation, which results in a smoother surface.

Figure 1(c) displays the Raman spectra recorded for NR and NR-CaP at room temperature, and in both cases there are peak shifts characteristic of natural rubber. For instance, the bands in the regions of 1665 cm^{-1} are attributed to stretching vibration C═O groups[28] and those at 2100 cm^{-1} are attributed to luminescence effects from nonrubber particles present in the natural rubber cream.[3,29] These effects are characteristic of materials that frequently exhibit a two-photon absorption capability with a wide range of vibrational modes and collective excitations.[30] The decrease in their intensity after the CaP incorporation is attributed to a decrease in the dispersion of the nonrubber particles, e.g., proteins and phospholipids, due to the process of migration from the surface to the CaP regions (see typical chemical color map—2900 cm^{-1} in the inset of the graphical abstract). A detailed explanation of this process can be found in ref 6.

Regarding the surface properties, Figure 1(d) shows a plot of $0.5\gamma_L(1 + \cos\theta)(\gamma^d_L)^{-1/2}$ versus $(\gamma^d_S/\gamma^d_L)^{1/2}$ for the determination of the dispersive $\gamma_S{}^d$ and polar $\gamma_S{}^p$ components of the free energy the from linear and angular coefficients, respectively. The values for the dispersive component $\gamma_S{}^d$ were 21.4 $mN{\cdot}m^{-1} \pm 0.01$ and 23.5 $mN{\cdot}m^{-1} \pm 0.01$ for NR and NR-CaP, respectively. This property is related to the dispersion interactions resulting from electron dipole fluctuations, which result in long distance forces. The presence of CaP particles induces a slight increase in $\gamma_S{}^d$, which characterizes both better stability and accommodation of the polymeric matrix. On the other hand, a marked difference between the polar components of NR and NR-CaP is evidenced, i.e., 1.94 ± 0.01 $mN{\cdot}m^{-1}$ and 1.27 ± 0.01 $mN{\cdot}m^{-1}$ for NR and NR-CaP, respectively, attributed to the migration of the charged (and luminescent) particles at the surfaces, which is corroborated by the Raman spectroscopy results (Figure 1(c)) and the decreasing of the negative charge surface from -44.1 ± 3.5 mV to -22.9 ± 1.6 mV as attested by zeta potential. The values for the solid tension γ_s were ~23.3 $mN{\cdot}m^{-1}$ and 24.8 $mN{\cdot}m^{-1}$ for NR and NR-CaP, respectively, calculated from approaches to polar−nonpolar liquids.[31] The results suggest that the surface was mainly modified by a change in the roughness, with $r_{NR} \approx 2r_{NR\text{-}CaP}$.

3.2. Stability of the Contact Line. The wetting properties of the NR surface were systematically investigated in the oral temperature range for implant dentistry purposes, taking into

DOI: 10.1021/acsbiomaterials.8b00723
ACS Biomater. Sci. Eng. 2018, 4, 2784−2793

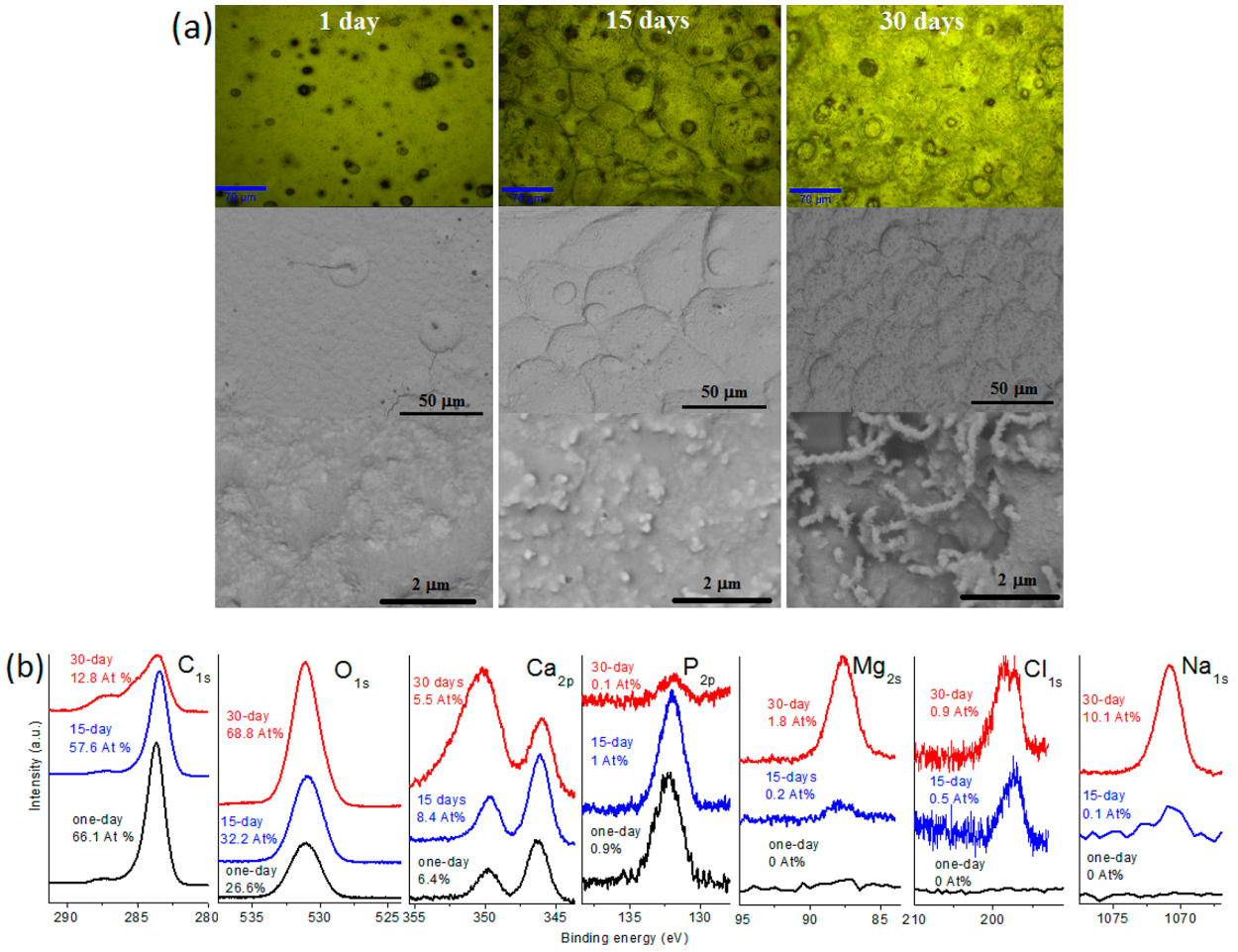

Figure 4. (a) Confocal microscopy images with contact angle data and scanning electron microscopy images at magnifications of 1000× and 30000×. (b) XPS spectra for the modified NR surfaces after exposure to a biological environment for different periods.

account the change in the roughness after CaP incorporation. The values for the equilibrium contact angle θ were 98°, 90°, and 84° for 20 °C, 37 °C, and 54 °C, respectively, indicating the hydrophobic property of the NR surface. The obtained same θ values for NR and NR-CaP at each temperature suggest that the morphology and wettability are independent in the roughness range of ∼20−37 nm. The solid−liquid tensions at the natural rubber surface were obtained for different temperatures, and the values are γ_{SL} [20 °C] ∼ 34 mN·m^{-1}, γ_{SL} [37 °C] ∼ 24 mN·m^{-1}, and γ_{SL} [54 °C] ∼ 16.5 mN·m^{-1}. The temperature influences both γ and γ_{SL}; hence, when the contact angle decreases, i.e., when the thermal energy at the interface is increased, the wettability of NR increases. The high solid−liquid tension (∼34 mN·m^{-1}) indicated the water-repellent property of the NR membranes. The comparison of the values is reported in Table 1.

The dynamic contact line of small drops on NR and NR-CaP was investigated. Figure 2 shows the typical evolution of the contact angles when liquid is added or removed from the drop. The advancing θ_a and receding θ_r contact angles on the NR surface as well as the different wettability regimes can thus be clearly identified: advance contact line (ACL), pinned contact line (PCL), and recede contact line (RCL). The RCL regime suggests a moderate pinning of the contact line. Based on the contact angle measurements, two parameters were determined: the dynamic contact angle hysteresis, $\Delta\theta_{dyn}$, and the pinning force (per unit length), defined as $F_{dyn} = \gamma(\cos\theta_r - \cos\theta_e)$,[32] with $\cos\theta_e = (\cos\theta_a + \cos\theta_r)\cdot 2^{-1}$. For the NR surface, the following values were obtained: $\Delta\theta_{dyn}$ = 17° and F_{dyn} = 9 mN·m^{-1}. The work of adhesion, defined as $W = \gamma(\cos\theta_{rup} - 1)$, was determined for both NR and NR-CaP surfaces, and the values obtained were 119 and 135 mJ·m^{-2}, respectively. The introduction of CaP should slightly increase the liquid−solid adhesion. The main parameters extracted from the wettability analysis are reported in Table 1. The hybridization of the NR polymer to obtain NR-CaP resulted in the change in the roughness with no change in the θ value. Such properties can be harnessed for the design of a stable biomaterial when the resistance of cell adhesion is an important factor as it avoids thrombotic responses.

3.3. Response to a Biological Environment. As mentioned above, the performance of a polymeric biomaterial is dependent on the contact between surfaces and the biological environment. Figures 3(a) and (b) show the micrographs of the surfaces of natural rubber before (NR) and after 1 day of (NR-SBF) exposure to a simulated body fluid. The NR surface appears to be sensitive to exposure to a biological environment, which implies both physical and chemical modifications. These changes result in a hydrophilization of the polymer surfaces as measured in range of θ from 90° close to 60° at 36 °C. The changes in the hydrophilicity after exposure of the surfaces to a biological environment can be explained by physicochemical modification of the polymer surface with the formation of clusters of

DOI: 10.1021/acsbiomaterials.8b00723
ACS Biomater. Sci. Eng. 2018, 4, 2784−2793

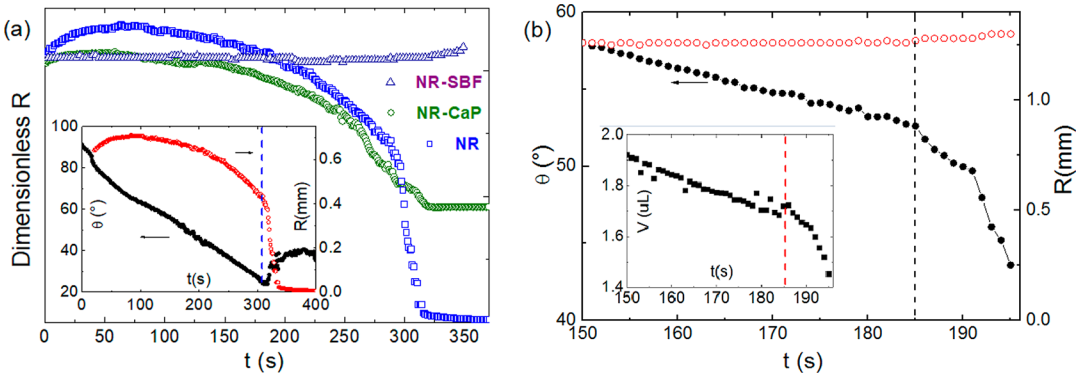

Figure 5. (a) Behavior of contact line: temporal evolution of dimensionless contact radius for NR, NR-CaP, and NR-SBF surfaces during evaporation of water droplets at 37 °C. Inset: temporal evolution of contact angle θ and contact radius R on NR surface. (b) Temporal evolution of contact angle θ and contact radius R on NR-SBF surface at 37 °C after a 30-day exposure to a biological environment with considerable changes in θ and the drop volume (inset) over time.

aggregated nanoparticles (insets of Figure 3). We also monitored the evolution of pH of the simulated biological environment around the NR sample over 1 day of the incubation process. The incubation process leads to a slight increase in the alkalinity of the fluid at 36 ± 1 °C.

Regarding the temporal evolution of the NR-SBF surface, Figure 4 shows images of the NR surfaces after 1, 15, and 30 days of exposure to a biological environment. The morphology of the surfaces and of the clusters of particles had different aspects after each period. However, an increase in the contact angle was observed during the period considered. These observations can be attributed to new coatings formed on the NR samples through the sequential absorption of ions onto the surface as the time of interaction with the biological environment progresses. The X-ray photoelectron spectra in Figure 4(b) show the variation in the chemical components on the NR surface as a function of contact time with the SBF. The spectra are characterized by a decrease in atomic carbon (%) and an increase in atomic oxygen (%) followed by an increase in atomic Mg, Na, and Cl (%) from 1 to 30 days. The overlapping of peaks observed in the Ca_{2p} spectrum after 30 days is attributed to the $Mg_{(KLL)}$ binding energy of around 350 eV. Therefore, the amount of the atomic calcium (%) was obtained from Ca_{2s}—438 eV. The increase in the chemical heterogeneity of the surface over time of interaction with SBF is associated with the surface charge and electric double layer. The negatively charged surface of the NR adsorbs preferentially positively charged ions, such as Ca^{2+}, followed by the adsorption of negatively charged ions, such as HPO_4^{2-}. As a result, different H^+ and OH^- groups become available on the surface over time, which explains the difference in the calcium concentrations for the three periods. A similar sequential ionic absorption has been previously observed in the XPS analysis of a titanium surface exposed to a biological environment for different periods,[33] which corroborates the phenomenology indicated in this study. In fact, three different coatings were formed on the NR-SBF surface, and the individual values of θ after different periods are no longer comparable.

3.4. Evaporation Kinetics. Experiments were performed on evaporation on the NR surface before and after exposure to biological environments (NR-SBF), and the contact angle and contact line were measured as a function of time. Qualitatively, it can be seen that the evaporation occurs according to the contact line between biofluids and surfaces. Figure 5(a) shows the evolution of the normalized contact radius during the drop evaporation on three surfaces: NR, NR-CaP, and NR-SBF. A similar behavior is observed on the NR and NR-CaP surfaces, where the contact line is initially pinned and then, at a certain time, it recedes. The presence of CaP particles does not seem to have a significant effect on the dynamics of the contact line on the surfaces. In contrast, on the NR-SBF surface, the line remained pinned during the whole evaporation process. This behavior can be attributed to the topographic and physicochemical modification of the surface (roughness, chemical heterogeneity, free energy, surface charge, etc.) induced by the exposure of NR samples to a biological environment. Figure 5(a), inset, shows the variation in the contact angle and contact radius during the evaporation process on the NR surface. Two distinct regimes can be identified: (i) the drop starts to evaporate with a decrease in θ and slight movements of the contact line attributed to accommodations in the drop area and (ii) the contact line starts to recede abruptly around 300 s (near the end of the evaporation process) suggesting a moderate pinning of the contact line. The depinning force due to evaporation arising at the transition is introduced as $F_{evap} = \gamma\Delta \cos \theta$[34] with $(\Delta \cos \theta)_{evap} = \cos \theta_{dep} - \cos \theta_i$. From the experimental data we found that $F_{evap} = 64$ mN·m^{-1}. A marked difference between dynamic and evaporation depinning forces ($F_{evap} \approx 6\ F_{dyn}$) was evidenced. Such a difference suggests that in the evaporation experiments a slight penetration of the liquid inside the surface features took place, increasing the liquid−solid interface and consequently the pinning effects on the contact line. The dependence of dynamic hysteresis on the sample history has been investigated in other systems, and a typical example is found in ref 35.

Figure 5(b) shows a drop evaporating on the NR-SBF surface after 30 days of exposure to the SBF. As can be seen, the drop starts to evaporate with a constant contact radius that is in the pinned contact line (PCL) regime. In this configuration, the contact angle gradually decreases. For this surface, the contact line did not overcome the pinning energy barrier to receding, which clearly indicates a complete Wenzel state[36] throughout the evaporation. According to the theory of drop evaporation, the drop volume is defined as $V(R,\theta) = (\pi R^3)(1 - \cos \theta)^2(2 + \cos \theta)(3 \sin^3 \theta)^{-1}$—its evolution is represented in the inset of Figure 5(b). A wetting transition was observed when the drops reached 1.7 μL (~185 s). The contact line remained pinned with an abrupt decrease in θ and $V(R,\theta)$. This phenomenon is characteristic of a time-depend-

DOI: 10.1021/acsbiomaterials.8b00723
ACS Biomater. Sci. Eng. 2018, 4, 2784−2793

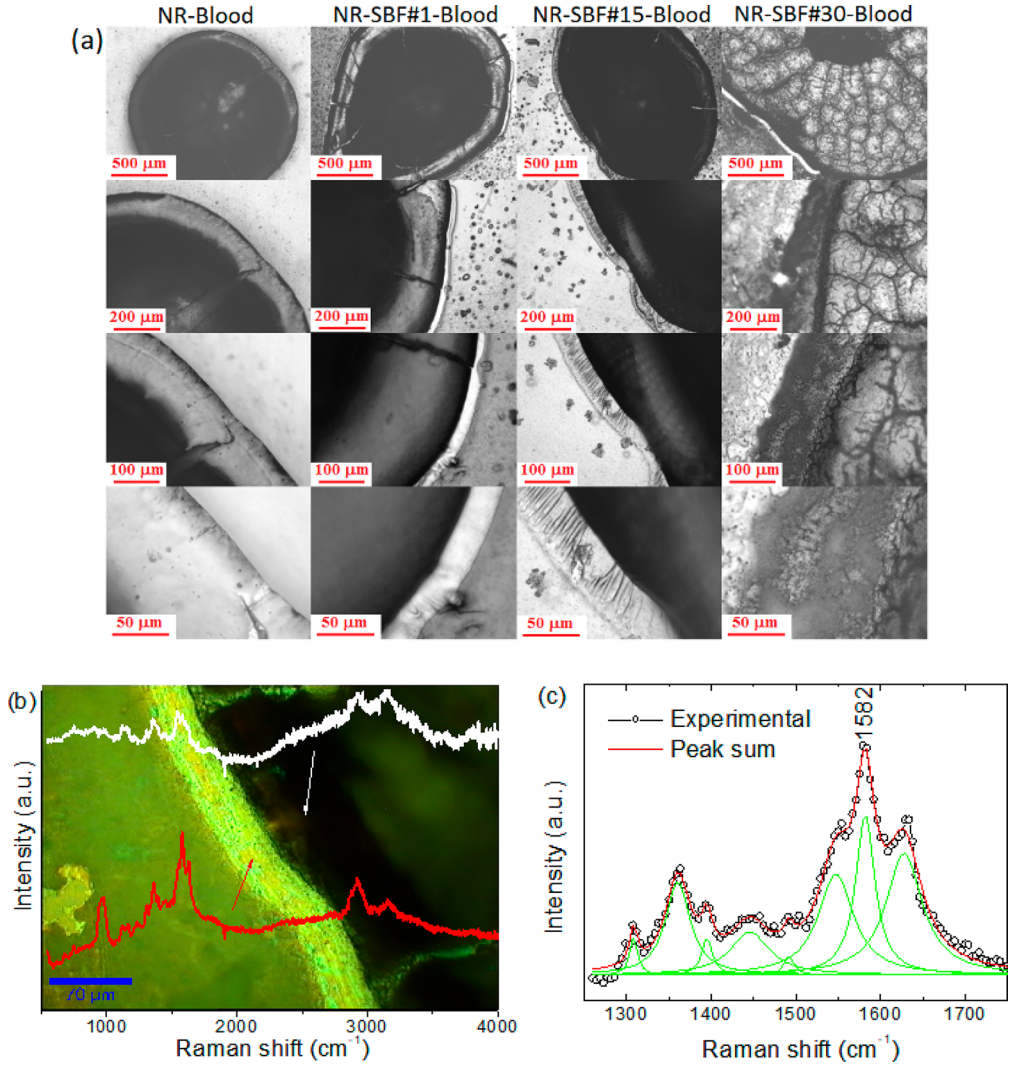

Figure 6. (a) Optical microscopy images (magnifications of 50×, 100×, 200×, and 500×) showing the morphologies of evaporated blood droplets (1 μL) at 37 °C on natural rubber (NR) surfaces and NR surfaces modified by exposure to SBF for different periods (1, 15, and 30 days). (b) Confocal image and Raman spectrum of blood stain ring on NR-SBF#30 surface obtained with λ = 514 nm and (c) line shape analyses of the Raman spectra.

ent wetting behavior,[37] which cannot be described by the conventional Wenzel model. In this scenario, a modification of the interfacial viscoelasticity can lead to a considerable change in θ over time.[38] Possible mechanisms responsible for the short-term effects on V and θ include the dissolution of biological salts on the surface, liquid flows from the droplet to the outside of the contact region, or an imbibition of the liquid at reentrances of the clusters of salt particles from the SBF (see last SEM image in Figure 4(a)). These mechanisms were detected in the hydrophilization range (within 30°−60°) for protein adsorption and cell adhesion.

3.5. Blood Wetting. The functionalization of the NR surface and its effects on the contact line with blood cells was investigated through an experiment involving evaporation of blood droplets on surfaces. The interfacial compatibility between blood and NR was correlated to the dispersive and polar components of the free energy of the NR surface using the values shown in section 3.1. The blood−surface tension is introduced as $\gamma_{SB} = \{(\gamma_B^P)^{1/2} - (\gamma_S^P)^{1/2}\}^2 + \{(\gamma_B^d)^{1/2} - (\gamma_S^d)^{1/2}\}^2$[39] where γ_B^P = 36.6 mN·m^{-1} and γ_B^d = 11.2 mN·m^{-1} are the polar and dispersive components of the surface energy of the blood, respectively. The optical microscopy images in Figure 6(a) show the morphology of blood droplets on the NR surfaces after the evaporation process. Different ringlike patterns were observed along the contact line, and these effects are attributed to the accumulation of the blood components at the self-pinned edge. A drop of blood on the NR surface is characterized by a uniform wetting of circular shape with a contact radius $R \sim 0.5$ mm and $\theta \sim 80°$. The high blood−surface tension (γ_{SB} = 23 mN·m^{-1}) and the hydrophobic characteristic of the NR surface ($\theta \sim 100°$) explain the suppression of the "coffee ring effects" which is associated with a low blood components adhesion and could be an interesting option for applications as an antifouling material for antithrombogenic implants.[40] In contrast, the drops of blood on the NR-SBF#1 and NR-SBF#15 surfaces exhibited nonuniform wetting with $R \sim 1$ mm and $\theta \sim 65°$ while the corresponding results for the NR-SBF#30 were high R (~1.5 mm) and low θ (~20°) values. In fact, the blood droplets appears to be very sensitive to NR-SBF#30. The crack pattern formed on such a surface has good agreement with the observations in a similar study[25] where blood had a contact

DOI: 10.1021/acsbiomaterials.8b00723
ACS Biomater. Sci. Eng. 2018, 4, 2784−2793

angle θ of 15°. This phenomenon has been attributed to the tensile stress developed through competition between adhesion at the interface and evaporation mechanisms. Moreover, the patterns observed in the images could be formed by capillary flow,[41] which also explains the contact line behaviors shown in Figure 5.

The characterization of the chemical phases of the adsorbed blood components on hybrid NR was obtained from the blood stain ring on NR-SBF#30. Figure 6(c) displays the Raman spectra of the molecular fingerprints of the contact line (ring) and interior of the blood drop. The Raman spectra exhibited characteristic bands of the hemoglobin macromolecular structure, regardless of the red blood cells (up >95% of the dried weight). For instance, the bands in the 2840−3000 cm^{-1} spectral range are assigned to C−H stretching from CH_2 and CH_3, the spectral region of phospholipidic chains, and characterized by symmetric and antisymmetric stretching modes enhanced by Fermi resonance.[42] Both erythrocytes and leucocytes exhibit bands from the CH_2 groups in this region. On the other hand, the Raman spectra of the contact line and interior of the drop exhibited some different characteristic bands. For instance, the prominent bands at the 1582−1590 cm^{-1} region are assigned to aromatic amino acids ($C\alpha Cm$ asymmetric stretching) of protein structures from blood, such as phenylalanine, tryptophan, and tyrosine. The Lorentzian decomposition of the spectra of the blood in this region is shown in Figure 6(c).We also report the presence of the bands at 1630 cm^{-1} (amide I) attributed to proteins and polypeptides, which come from peptide bonds.[43] In addition, the high intensity of the Raman peaks at 1582 cm^{-1} suggests that the red blood cells are in an oxygenated state[44] at the contact line with the NR-SBF#30 surface. From a material science perspective, NR surfaces are activated by the spontaneous growth of apatite accompanied by the consumption of calcium and phosphate ions inducing a nonrubber phase. The new phases formed on NR surfaces after interaction with SBF can have various positive ions, for example, Ca^{2+} and PO_4^{3-}, chemical groups responsible to decrease the negative charges from −44.1 ± 3.5 to −15.1 ± 1.2 mV, as attested by the zeta potential. The resulting negative charge is slightly lower than a cell membrane, which consists of phospholipid bilayers with charge ∼ −20 mV. Therefore, the hybrid NR-SBF can induce blood wettability by adsorbing blood components. Such finding enables the polymer natural rubber to new steps toward biomedical application because the slightly negatively charged molecules show a lower unfavorable effect on cell response.[45]

4. CONCLUSION

A study on the wettability of the surface of natural rubber (NR) with a view to its application as a biomaterial was conducted. The hydrophobic characteristic of the NR surface associated with high blood-surface tension can be an interesting option for applications when a poorly protein/cell-adhesion is required. Examples include hemodialysis membranes, stents, artificial blood vessels, heart valves, and stents. The incorporation of calcium phosphate particles into the polymer (hybrid NR-CaP surface) modified the roughness and decreased the negative surface charge with no change in θ. After exposure to the simulated biological environment, particles originating from fluid grew spontaneously on the NR surfaces, increasing the formation of apatite with the consumption of the calcium and phosphate ions. Such a process leads to values of negative surface charge lower than cell membrane. The new NR-SBF surface obtained after the biomineralization process exhibited a pinned contact line regime, a wetting transition within the θ range of protein-cell adsorption, and an increase in the wettability of blood. The pinned contact line between the blood and NR-SBF surface left behind biomolecules with thick edges along the interface, evidencing the "coffee ring effect". The chemical characterization of the blood fingerprints indicated that aromatic amino acids of the proteins are involved in the adsorption process on the hybrid NR surface. The practicality in modifying the hydrophobic−hydrophilic characteristics make this natural polymer a candidate for tissue engineering, for instance, a flexible scaffold taking advantage of the mechanical properties of the NR, the bioactive properties of the bioceramics, and the modulation of surface charge by a hybridization process.

■ ASSOCIATED CONTENT

Supporting Information

The Supporting Information is available free of charge on the ACS Publications website at DOI: 10.1021/acsbiomaterials.8b00723.

Table S1 shows data on the quality of the human blood samples according to protocols approved by the ethics committee of the institution. Table S2 shows values of surface zeta-potential (ζ) at pH 7.4, 25 °C measured three times for NR, NR-CaP, and NR-SBF samples. Table S3 shows the statistical data on the surface area obtained from AFM in different regions of NR and NR-CaP samples. Table S4 shows values for contact angle θ obtained from droplets on NR and NR-CaP surfaces NR. (PDF)

■ AUTHOR INFORMATION

Corresponding Author

*E-mail: rodneymn@ifsc.usp.br.

Notes

The authors declare no competing financial interest.

■ ACKNOWLEDGMENTS

The authors thank the Growth of Crystals and Ceramic Materials team of the Universidade de São Paulo and are indebted to Dr. Amauri Jardim de Paula and Naiara Cipriano of the Universidade Federal do Ceara, Lilian Reschini of the São Francisco analyze center, and Dr. Ana Paula Ramos and Dr. Pietro Ciancaglini of the Laboratório de Físico-Química de Superfícies e Colóides for all support in the experiments with simulated body fluid, blood, and zeta potential analysis, respectively. This work was supported by the Brazilian Agency FAPESP, grant number 2013/21970-8.

■ REFERENCES

(1) Teo, A.; Mishra, A.; Park, I.; Kim, Y. J.; Park, W. T.; Yoon, Y. J. Polymeric Biomaterials for Medical Implants and Devices. *ACS Biomater. Sci. Eng.* **2016**, *2* (4), 454−472.

(2) Ma, Z.; Mao, Z.; Gao, C. Surface modification and property analysis of biomedical polymers used for tissue engineering. *Colloids Surf., B* **2007**, *60*, 137−157.

(3) Nascimento, R. M.; Faita, F. L.; Agostini, D. L. S.; Job, A. E.; Guimarães, F. E. G.; Bechtold, I. H. Production and characterization of natural rubber-Ca/P blends for biomedical purposes. *Mater. Sci. Eng., C* **2014**, *39*, 29−34.

DOI: 10.1021/acsbiomaterials.8b00723
ACS Biomater. Sci. Eng. 2018, 4, 2784−2793

(4) Floriano, J. F.; Mota, L. S.; Furtado, E. L.; Rossetto, V. J.; Graeff, C. F. Biocompatibility studies of natural rubber latex from different tree clones and collection methods. *J. Mater. Sci.: Mater. Med.* **2014**, *25*, 461−470.
(5) Borges, F. A.; Barros, N. R.; Garms, B. C.; Miranda, M. C. R.; Gemeinder, J. L. P.; Ribeiro-Paes, J. T.; Silva, R. F.; Toledo, K. A.; Herculano, R. D. Application of natural rubber latex as scaffold for osteoblast to guided bone regeneration. *J. Appl. Polym. Sci.* **2017**, *134*, 45321.
(6) Moura, J. M. L.; Ferreira, J. F.; Marques, L.; Holgado, L.; Graeff, C. F. O.; Kinoshita, A. Comparison of the performance of natural latex membranes prepared with different procedures and PTFE membrane in guided bone regeneration (GBR) in rabbits. *J. Mater. Sci.: Mater. Med.* **2014**, *25*, 2111−20.
(7) Rupp, F.; Gittens, R. A.; Scheideler, L.; Marmur, A.; Boyan, B. D.; Schwartz, Z.; Geis-Gerstorfer, J. G. A Review on the Wettability of Dental Implant Surfaces: Theoretical and Experimental Aspects. *Acta Biomater.* **2014**, *10*, 2894−2906.
(8) Gittens, R. A.; Scheideler, L.; Rupp, F.; Hyzy, S. L.; Geis-Gerstorfer, J.; Schwartz, Z.; Boyan, B. D. A Review on the Wettability of Dental Implant Surfaces II: Biological and Clinical Aspects. *Acta Biomater.* **2014**, *10*, 2907−2918.
(9) Shabalovskaya, S. A.; Siegismund, D.; Heurich, E.; Rettenmayr, M. Evaluation of wettability and surface energy of native Nitinol surfaces in relation to hemocompatibility. *Mater. Sci. Eng., C* **2013**, *33*, 127−32.
(10) Park, J. H.; Wasilewski, C. E.; Almodovar, N.; Olivares-Navarrete, R.; Boyan, B. D.; Tannenbaum, R.; Schwartz, Z. The responses to surface wettability gradients induced by chitosan nanofilms on microtextured titanium mediated by specific integrin receptors. *Biomaterials* **2012**, *33*, 7386−7393.
(11) Dowling, D. P.; Miller, I. S.; Ardhaoui, M.; Gallagher, W. M. Effect of surface wettability and topography on the adhesion of osteosarcoma cells on plasma-modified polystyrene. *J. Biomater. Appl.* **2011**, *26*, 327−47.
(12) Rosales-Leal, J. I.; Rodríguez-Valverde, M. A.; Mazzaglia, G.; Ramón-Torregrosa, P. J.; Díaz-Rodríguez, L.; García-Martínez, O.; Vallecillo-Capilla, M.; Ruiz, C.; Cabrerizo-Vílchez, M. A. Effect of roughness, wettability and morphology of engineered titanium surfaces on osteoblast-like cell adhesion. *Colloids Surf., A* **2010**, *365*, 222−229.
(13) Ranella, A.; Barberoglou, M.; Bakogianni, S.; Fotakis, C.; Stratakis, E. Tuning cell adhesion by controlling the roughness and wettability of 3D micro/nano silicon structures. *Acta Biomater.* **2010**, *6*, 2711−2720.
(14) Arima, Y.; Iwata, H. Effect of wettability and surface functional groups on protein adsorption and cell adhesion using well-defined mixed self-assembled monolayers. *Biomaterials* **2007**, *28*, 3074−3082.
(15) Nascimento, R. M.; Carvalho, V. R.; José Silvio Govone, J. S.; Hernandes, A. C.; Cruz, N. C. Effects of negatively and positively charged Ti metal surfaces on ceramic coating adhesion and cell response. *J. Mater. Sci.: Mater. Med.* **2017**, *28*, 28−33.
(16) Li, Y.; Wei, Y.; Liao, J.; Hao, Y.; Ning, C.; Jiang, L.; Wang, S. Surface Wettability Switched Cell Adhesion and Detachment on Conducting Polymer Nano array. *Adv. Mater. Interfaces* **2016**, *3*, 1600598.
(17) Gentleman, M. M.; Gentleman, E. The role of surface free energy in osteoblast−biomaterial interactions. *Int. Mater. Rev.* **2014**, *59* (8), 417−429.
(18) Zhao, G.; Raines, A.; Wieland, M.; Schwartz, Z.; Boyan, B. D. Requirement for both micro-and submicron scale structure for synergistic responses of osteoblasts to substrate surface energy and topography. *Biomaterials* **2007**, *28* (18), 2821.
(19) Nakamura, M.; Nagai, A.; Hentunen, T.; Salonen, J.; Sekijima, Y.; Okura, T.; Hashimoto, K.; Toda, Y.; Monma, H.; Yamashita. Surface Electric Fields Increase Osteoblast Adhesion through Improved Wettability on Hydroxyapatite Electret. *ACS Appl. Mater. Interfaces* **2009**, *1* (10), 2181−2189.
(20) Rungsiyakull, C.; Li, Q.; Sun, G.; Li, W.; Swain, M. V. Surface morphology optimization for osseointegration of coated implants. *Biomaterials* **2010**, *31* (27), 7196−7204.
(21) Hallab, N. J.; Bundy, K. J.; O'Connor, K.; Moses, R. L.; Jacobs, J. J. Evaluation of Metallic and Polymeric Biomaterial Surface Energy and Surface Roughness Characteristics for Directed Cell Adhesion. *Tissue Eng.* **2001**, *7*, 55.
(22) Molina, M. P.; Moreno, P. G.; Barbero, J. E. F.; O'Valle, F.; Reyes, A. B. J.; Vinuesa, J. L. O.; Torregrosa, P. J. R. Role of wettability and nanoroughness on interactions between osteoblast and modified silicone surfaces. *Acta Biomater.* **2011**, *7*, 771−778.
(23) Grundke, K.; Augsburg, A. On the determination of the surface energetics of porous polymer materials. *J. Adhes. Sci. Technol.* **2000**, *14*, 765.
(24) Xu, W.; Choi, C. From sticky to slippery droplets: dynamics of contact line depinning on superhydrophobic surfaces. *Phys. Rev. Lett.* **2012**, *109*, 024504-1−4.
(25) Sobac, B.; Brutin, D. Desiccation of a sessile drop of blood: Cracks, folds formation and delamination, Colloids and Surfaces A: Physicochem. *Colloids Surf., A* **2014**, *448*, 34−44.
(26) Kokubo, T.; Takadama, H. How useful is SBF in predicting in vivo bone bioactivity? *Biomaterials* **2006**, *27*, 2907−2915.
(27) Faita, F. L.; Dotto, M. E. R.; França, L. G.; Cabrera, F. C.; Job, A. E.; Bechtold, I. H. Characterization of natural rubber membranes using scaling laws analysis. *Eur. Polym. J.* **2014**, *50*, 249−254.
(28) Simoes, R. D.; Job, A. E.; Chinaglia, D. L.; Zucolotto, V.; Camargo-Filho, J. C.; Alves, N.; Giacometti, J. A.; Oliveira, O. N., Jr; Constantino, C. J. L. Structural h:characterization of blends containing both PVDF and natural rubber latex. *J. Raman Spectrosc.* **2005**, *36*, 1118−1124.
(29) Sansatsadeekul, J.; Sakdapipanich, J.; Rojruthai, P. Characterization of associated proteins and phospholipids in natural rubber latex. *J. Biosci. Bioeng.* **2011**, *111*, 628−634.
(30) Drobizhev, M.; Makarov, N. S.; Tillo, S. E.; Hughes, T. E.; Rebane, A. Two-photon absorption properties of fluorescent proteins. *Nat. Methods* **2011**, *8*, 393−399.
(31) Owens, D. K.; Wendt, R. C. Estimation of the Surface Free Energy of Polymers. *J. Appl. Polym. Sci.* **1969**, *13*, 1741−1747.
(32) Joanny, J. F.; de Gennes, P. G. A model for contact angle hysteresis. *J. Chem. Phys.* **1984**, *81*, 552−562.
(33) Kokubo, T.; Yamaguchi, S. Bioactive Titanate Layers Formed on Titanium and Its Alloys by Simple Chemical and Heat Treatments. *Open Biomed. Eng. J.* **2015**, *9* (Suppl 1−2), 29−41.
(34) Chen, X.; Ma, R.; Li, J.; Hao, C.; Guo, W.; Luk, B. L.; Li, S. C.; Yao, S.; Wang, Z. Evaporation of droplets on superhydrophobic surfaces: surface roughness and small droplet size effects. *Phys. Rev. Lett.* **2012**, *109*, 116106.
(35) Nascimento, R. M.; Cottin-Bizonne, C.; Pirat, C.; Ramos, S. M. M. Water Drop Evaporation On Mushroom-like Superhydrophobic Surface: temperature effects. *Langmuir* **2016**, *32* (8), 2005−2009.
(36) Wenzel, R. N. Resistance of solid surfaces to wetting by water. *Ind. Eng. Chem.* **1936**, *28*, 988.
(37) Mishra, H.; Schrader, A. M.; Lee, D. W.; Gallo, A., Jr; Chen, S. Y.; Kaufman, Y.; Das, S.; Israelachvili, J. N. Time-Dependent Wetting Behavior of PDMS Surfaces with Bioinspired, Hierarchical Structures. *ACS Appl. Mater. Interfaces* **2016**, *8* (12), 8168−8174.
(38) Style, R. W.; Hyland, C.; Boltyanskiy, R.; Wettlaufer, J. S.; Dufresne, E. R. Surface Tension and Contact with Soft Elastic Solids. *Nat. Commun.* **2013**, *4*, 1.
(39) Chen, J. Y.; Leng, Y. X.; Tian, X. B.; Wang, L. P.; Huang, N.; Chu, P. K.; Yang, P. Antithrombogenic investigation of surface energy and optical bandgap and hemocompatibility mechanism of Ti $(Ta^{+5})O_2$ thin films. *Biomaterials* **2002**, *23*, 2545−2552.
(40) Liu, X.; Yuan, L.; Li, D.; Tang, Z.; Wang, Y.; Chen, G.; Chen, H.; Brash, J. L. Blood Compatible Materials: State of the Art. *J. Mater. Chem. B* **2014**, *2*, 5718−5738.
(41) Deegan, R. D.; Bakajin, O.; Dupont, T. F.; Huber, G.; Nagel, S. R.; Witten, T. A. Capillary flow as the cause of ring stains from dried liquid drops. *Nature* **1997**, *389* (6653), 827−829.

DOI: 10.1021/acsbiomaterials.8b00723
ACS Biomater. Sci. Eng. 2018, 4, 2784−2793

(42) Gaber, B. P.; Peticolas, W. L. On the quantitative interpretation of biomembrane structure by Raman spectroscopy. *Biochim. Biophys. Acta, Biomembr.* **1977**, *465*, 260.
(43) Barth, A. Infrared spectroscopy of proteins. *Biochim. Biophys. Acta, Bioenerg.* **2007**, *1767*, 1073−1101.
(44) Perozziello, G.; Candeloro, P.; De Grazia, A.; Esposito, F.; Allione, M.; Coluccio, M. L.; Tallerico, R.; Valpapuram, I.; Tirinato, L.; Das, G.; Giugni, A.; Torre, B.; Veltri, P.; Kruhne, U.; Valle, G. D.; Fabrizio, E. D. Microfluidic device for continuous single cells analysis via Raman spectroscopy enhanced by integrated plasmonic nanodimers. *Opt. Express* **2016**, *24* (2), A180−A190.
(45) Xiao, K.; Li, Y.; Luo, J.; Lee, J. S.; Xiao, W.; Gonik, A. M.; Agarwal, R. G.; Lam, K. S. The effects of surface charge on *in vivo* biodistribution of PEG-oligocholic acid based micellar nanoparticles. *Biomaterials* **2011**, *32*, 3435.

DOI: 10.1021/acsbiomaterials.8b00723
ACS Biomater. Sci. Eng. 2018, 4, 2784−2793